JOURNAL OF BIOMOLECULAR STRUCTURE AND DYNAMICS
https://doi.org/10.1080/07391102.2022.2045220



# Single-walled silicon nanotube as an exceptional candidate to eliminate SARS-CoV-2: a theoretical study

Pedro Simão Sousa Mendonça[a], Jeziel Rodrigues dos Santos[a,b], Osmair Vital de Oliveira[c], José Divino dos Santos[a] and Elson Longo[b]

[a]LQTAM, Goiás State University, GO, Brazil; [b]Chemistry Department, CDMF, LIEC, Federal University of São Carlos, São Carlos, Brazil; [c]Federal Institute of Education, Science and Technology of São Paulo, Catanduva Campus, Catanduva, SP, Brazil

Communicated by Ramaswamy H. Sarma

**ABSTRACT**

In this work, computational chemistry methods were used to study a silicon nanotube ($Si_{192}H_{16}$) as possible virucidal activity against SARS-CoV-2. This virus is responsible for the COVID-19 disease. DFT calculations showed that the structural parameters of the $Si_{192}H_{16}$ nanotube are in agreement with the theoretical/experimental parameters reported in the literature. The low energy gap value (0.29 eV) shows that this nanotube is a semiconductor and exhibits high reactivity. For nanomaterials to be used as virucides, they need to have high reactivity and high inhibition constant values. Therefore, the adsorption of $^3O_2$ and $H_2O$ on the surface of $Si_{192}H_{16}$ ($Si_{192}H_{16}@O_2$-$H_2O$) was performed. In this process, the formation and activation energies were −51.63 and 16.62 kcal/mol, respectively. Molecular docking calculations showed that the $Si_{192}H_{16}$ and $Si_{192}H_{16}@O_2H$-OH nanotubes bind favorably on the receptor-binding domain of the SARS-CoV-2 spike protein with binding energy of −11.83 (Ki = 2.13 nM) and −11.13 (Ki = 6.99 nM) kcal/mol, respectively. Overall, the results obtained herein indicate that the $Si_{192}H_{16}$ nanotube is a potential candidate to be used against COVID-19 from reactivity process and/or steric impediment in the S-protein.

**ARTICLE HISTORY**
Received 30 November 2021
Accepted 17 February 2022

**KEYWORDS**
COVID-19; virus inactivation; surface functionalization; antiviral surfaces; silicon nanotubes; theoretical methods

## 1. Introduction

In late December 2019, contamination in humans by a novel coronavirus causing severe acute respiratory syndrome (SARS) was reported in Wuhan, Hubei Province, China. Where, the first official hospitalization was reported on December 12, 2019 and rapidly it was declared as a pandemic with a high spread rate, becoming a serious global public health threat (Wolfe et al., 2007).

Fan Wu *et al.* (Wu et al., 2020), were the first researchers to report in the literature a case study of a 41-year-old patient admitted to Wuhan Central Hospital on December 26, 2019. The results showed that the broncho alveolar fluid contained a virus whose genome had a strong phylogenetic relationship to the coronaviruses that cause SARS and MERS (Middle East Respiratory Syndrome). The virus initially known as WH Human coronavirus 1 (WHCV), then 2019-nCoV and finally SARS-CoV-2 showed 89.1% genomic similarity with Bat SL CoVZC45, a virus resulting from a bat collected in China (Hu et al., 2018).

Since then, some 254 mi people worldwide have been infected and deaths have exceeded 5.11 mi. Fatigue, fever, headache, runny nose, and dry cough are the main clinical symptoms of COVID-19 (Larsen et al., 2020). So far, no effective antiviral drugs have been reported in the literature, with vaccination being the most effective means against the spread and genetic mutation of the virus.

The most common mechanism of contamination shows that SARS-CoV-2 can be transmitted by human-to-human contact, through respiratory droplets at short distance or even by contact on contaminated surfaces, since studies report that the survival of the virus on surfaces depends on several factors such as the type of surface, temperature, environmental humidity and specific strain of the virus, and can vary in a range of 2 to 216 hours (Kampf et al., 2020).

Considering this scenario, the development of new materials with virucidal capabilities is very important and emergent. In this way, theoretical and experimental researchers are joining forces to find viable solutions to prevent the transmission, spread, and entry of new COVID-19 pathogens into the human body. One of the results of this theoretical-experimental synergy was recently published by our research group, where we report the development of a mask, a personal protective equipment (PPE), composed of nanoparticles of an EVA-$SiO_2$-Ag polymeric composite. The tests performed indicated high antibacterial activity for *Escherichia coli* (*E. coli*) and *Staphylococcus aureus* (*S. aureus*), as well as for SARS-CoV-2 (Assis et al., 2021). Quantum mechanics calculations propose a simple mechanism, where the amorphous silica (a-$SiO_2$), with band gap of approximately 2.0 eV is used as

CONTACT Jeziel Rodrigues dos Santos prof.jeziel@gmail.com
P.S.S.M and J.R.S contributed equally.
Supplemental data for this article can be accessed online at https://doi.org/10.1080/07391102.2022.2045220.

a catalytic material for the production of protonated superoxide radicals ($O_2H^*$) and hydroxyl radicals ($OH^*$) that are strong oxidizing agents.

Besides personal protection equipments, packaging films for the protection of consumer products such as fruits and vegetables were produced using the PVC-$SiO_2$-Ag composite, and demonstrated 99.8% effectiveness in eliminating fungus, bacteria (*Taphylococcus aureus, Escherichia coli, Penicillium funiculosum*) and viruses (SARS-CoV-2) by surface contact of 2 hours and 15 minutes (Assis et al., 2021). The improved bactericidal and virucidal activity of these materials is evidenced through the plasmonic effect, caused by the presence of Ag in the composite, which becomes the main reaction channel generating reactive oxygen species (ROS) on the surface.

Reactive oxygen species (ROS) is a collective term describing products formed from the incomplete reduction of oxygen and includes the formation of superoxide anion ($^1O_2\bullet^-$) and its protonated form ($HO_2\bullet^-$), hydrogen peroxide ($H_2O_2$), singlet oxygen ($^1O_2$) and hydroxyl radicals ($OH^-$) (Burwell, 1966; Gligorovski et al., 2015; Hayyan et al., 2016; Kearns, 1971; Lissi et al., 1993; Nosaka & Nosaka, 2017; B. Yang et al., 2019). It is now known that several semiconductors, of various morphologies, can be used as catalytic precursors in the formation of ROS. The functionality of these semiconductors was proposed by Fujishima and Honda who first reported titanium oxide ($TiO_2$) nanoparticles as a photocatalyst for water splitting (• OH, • Honda et al., 1998), whereby, the processes of hydroxyl radical production involved on the surface were gradually recognized and elucidated in the subsequent decades (Nosaka & Nosaka, 2016). Once formed on the surface of materials, ROS can have distinct redox properties, they are reducing agents, such as superoxide ($O_2^-$) or act as oxidizing agents, such as hydrogen superoxide ($O_2H$).

The discovery and synthesis of carbon nanotubes (Iijima, 1991) with metallic properties and semiconductor or insulating material (depending on their chirality) (Hirana et al., 2013) were fundamental to the development and applications of this new class of nanomaterials. The applications of carbon nanotubes, based on theoretical and experimental studies, range from support in heterogeneous catalysis (Planeix et al., 1994), lithium ion battery anode material (De Las Casas & Li, 2012), drug carriers (Zhang et al., 2011), water treatment (Ma et al., 2017), gas sensors, such as, $SF_6$, $NO_2$, $H_2S$, $H_2$, $CO_2$, $CH_4$, CO and $H_2O_2$ (Camilli & Passacantando, 2018; Han et al., 2019; Sharafeldin & Allam, 2017; Wang et al., 2018), as well as in the study of materials with virucidal capacity (Aasi et al., 2020), where, recently, Aref Aasi *et al.,* reported the results of a theoretical study of the surface functionalization of carbon nanotubes decorated with Pt, Rh, Ru and Cu single-walled with $H_2O_2$ as excellent candidates in the development of antiviral surfaces, since the adsorption results on the decorated nanotubes proved to be extremely spontaneous.

In search of new materials that can achieve similar applications, the so-called inorganic nanotubes (Serra et al., 2019) have emerged as a viable alternative for replacing carbon nanotubes, since most of the electronic properties are independent of their chirality (Sadan et al., 2008). Among the inorganic nanotubes that have wide application in different areas, we can cite boron nitride nanotubes (BNNT) (dos Santos et al., 2020; Golberg et al., 2007; Solimannejad & Noormohammadbeigi, 2017), zirconium oxide nanotubes (ZNT) (Antônio Pinheiro Lobo et al., 2020; Berger et al., 2008), titanium oxide nanotubes ($TiO_2$NT) (Jitianu et al., 2004), as well as structures composed of atoms belonging to the same carbon group, such as germanium nanotubes (GeNT's) (Seifert et al., 2001) and silicon nanotubes (SiNTs) (Fagan et al., 2000). Among them, SiNT's have zigzag conformation and are promising structures for the composition of semiconductor materials, because they have band gaps smaller than 2.0 eV (Bai et al., 2004; X. Yang & Ni, 2005) which characterizes it as a good semiconductor.

The synthesis of SiNT's is not energetically favorable in comparison with carbon nanotubes, due to the tendency of Si-Si bonds to form $sp^3$-type hybridizations and not $sp^2$-type ones, as occurs with C-C bonds in CNT's (Fagan et al., 2000; Röthlisberger et al., 1994). SiNTs can be synthesized in porous Alumina ($Al_2O_3$) supported by molecular beams (Jeong et al., 2003), or also by gas condensation techniques (Castrucci et al., 2006) has been applied mainly in energy storage studies (Pokatilov et al., 2005; Song et al., 2010; Yoo et al., 2012).

To better understand the properties of nanostructured materials, both the changes caused by functionalization and formation of root species on the surface, computational simulation by means of density functional theory (DFT) presents a practical and effective solution. For example, recently Mohammad Solimannejad and Motahareh Noormohammadbeig (Solimannejad & Noormohammadbeigi, 2017) used DFT to investigate the sensing ability of boron nitride nanotubes for hydrogen superoxide ($HO_2$) root species. As a result, the adsorption process proved to be energetically favorable and the significant changes in the boundary orbital regions (HOMO and LUMO) show that BNNT can be used as a chemical sensor for this root species.

Although quantum mechanical methods are essential for the structural and electronic characterization of small nanotubes, they are not able to predict their interaction with macromolecules, such as proteins, due to the high computational cost. The identification of the interaction region between a nanotube and a protein is of great importance to identify the amino acids involved in chemical processes, for example oxidation. In this scope, molecular docking method is one of the most used approaches to predict the nanotube-protein interaction. In this way, Gonzalez-Durruthy (González-Durruthy et al., 2017) performed docking calculations to obtain the interaction of functionalized single wall carbon nanotube regions (SWCNT-H, SWCNT-OH, SWCNT-COOH) with different VDAC (voltage dependent anion channel) structures. In this study, SWCNT-COOH was the complex that showed the highest interaction strength with VDACs. In another work, Lu (N. Lu et al., 2018) studied the interaction of fibrinogen protein (fibrinogen) with SWCNTs via molecular docking, and the π-π interactions were responsible by the highest contribution in the SWCNTs-fibrinogen interactions. Where the SWCNTs interact with the following residues:

ASP203, LYS206, ASN243, GLU245, ASN246, LYS323, ARG346, VAL347, TYR348, TYR349, SER358, THR359, and PRO360. Regarding COVID-19, Patel et. al (Patel et al., 2021) used the docking method to study the interaction between MWCNTs (multi-walled carbon nanotubes) and the SARS-CoV-2 Spike protein (S-protein). Overall, their results show favorable interaction between MWCNTs and the S-protein.

Based on these considerations, herein, DFT method was used to study the functionalization of the $H_2O$ and $^3O_2$ species on the single-walled SiNTs surface in zigzag conformation. In addition, molecular docking calculations were performed to predict the nanotube-protein interaction, where the favorable interaction of them are essential for the virucidal application. It is worth noting that so far, no experimental and/or theoretical studies reporting the mechanism of surface functionalization of SiNT's in the presence of $H_2O$ and $^3O_2$ have been found in the literature. Also, we did not find works reporting the interaction between SiNT's and the SARS-CoV-2 S-protein. Therefore, the present work may contribute to the development of new antiviral surfaces as well as in the understanding of SiNT's-Spike protein interactions.

## 2. Computational details

### 2.1. Quantum chemistry methods

The initial structure of the (8,0) SiNT model consisting of 192 Si atoms was constructed in Cartesian coordinates using an internal script that can be consulted in the Supplementary Materials (see Supplementary Material S.1). The terminal atoms were saturated by 16 hydrogen atoms to avoid boundary effects, forming the compound $Si_{192}H_{16}$. This nanotube model is 10.61 and 37.98 Å in diameter and length, respectively. For the $Si_{192}H_{16}@O_2$ complex, it was constructed by positioning the $O_2$ molecule in different regions of the nanotube, positioning it at different angles (90° and 180°) in relation to the surface, (see Figure 2). For the $Si_{192}H_{16}@O_2H$-OH complex, the oxygen belonging to the water molecule was placed under the surface to hear the Si105-O3 interaction, so that the hydrogen belonging to the water can be free to interact with the already functionalized $O_2$ molecule, (see Figure 2). All complexes were initially optimized with semi-empirical PM7 (Stewart, 2013) using the open source software MOPAC2016 (James JP Stewart, 1990). Posteriorly, the structure with minimum energy was reoptimized with DFT calculations considering the hybrid functional B3LYP (Dobbs & Hehre, 1986) with Pople basis set 6-31 G* (Rassolov et al., 2001). This procedure was chosen to balance the computational cost and the quality of the results. In addition, some works reported in the literature show that this level of theory is sufficient to describe nanotubes that have Si in their composition (Mahdavifar et al., 2013; Soltani et al., 2013). The stationary points were defined as a minimum energy point using the harmonic vibrational states, in which no negative frequencies were observed. All DFT calculations were performed in vacuum using the Gaussian09 (Frisch, 2009). The natural orbital bonding (NBO) method (Glendening et al., 2012) was used to calculate the atomic charges. The scattering interaction correction was taken into account using Grimme's method (GD3) (Grimme et al., 2010). Partial density of states (PDOS) analysis was performed using an in-house script (see Supplementary Material S.2). The binding order was obtained and analyzed by means of the computational package Multiwfn (T. Lu & Chen, 2012). The adsorption energy ($E_{ad}$) of $O_2$ ($Si_{192}H_{16}@O_2$) and the formation energy ($E_{form}$) of the $Si_{192}H_{16}@O_2H$-OH compound was calculated using equations 1 and 2, respectively.

$$E_{ad} = E_{SiNT@O2} - (E_{SiNT} + E_{O2}) \quad (1)$$

$$E_{form} = E_{SiNT@O2H-OH} - (E_{SiNT@O2} + E_{H2O}) \quad (2)$$

where $E_{SiNT@O2}$ is the total energy of the $Si_{192}H_{16}@O_2$ complex, $E_{SiNT}$ is the total energy of $Si_{192}H_{16}$, $E_{O2}$ is the total energy of molecular oxygen in the triplet state, $E_{SiNT@O2H-OH}$ is the total energy of the $Si_{192}H_{16}@O_2H$-OH complex, and $E_{H2O}$ is the total energy of water.

### 2.2. Molecular docking

The initial structure of the Spike protein (S-protein) isolated from SARS-CoV-2 was obtained from the S-protein@ACE2 complex elaborated by Shah *et al.* (Shah et al., 2020). The AutoDockTools software (ADT) (Allouche, 2011) was used to prepare the S-protein and nanotubes in PDBQT format, which contains the structural and electrostatic data of the compounds. The grid of electrostatic interactions between the enzyme and the nanotubes was determined by the program AutoGrid4 (Allouche, 2011). The grid dimensions were fixed at $72 \times 86$ x 54 points centered at $91.411 \times 112.34 \times 67.085$ Å and with a spacing of 1.0 Å. This grid was sufficient to cover all the atoms of the receptor binding domain (RBD) of the S-protein, and this is the binding region for Human ACE2. For the nanotubes (SiNT and SiNT@$O_2$H-OH), the charges were obtained from semi-empirical calculations with PM7 Hamiltonian (Stewart, 2013) from the MOPAC2016 program (James J. P. Stewart, 1990). All docking calculations were performed in AutoDock4 (Allouche, 2011) . In these calculations, the S-protein was considered rigid and the nanotubes flexible. The parameters used in the docking calculations were those standardized in the AutoDock4 program (Allouche, 2011), except for the number of runs, which were 20 for each nanotube.

## 3. Results and discussion

### 3.1. Silicon nanotubes (8,0)

The optimized structure and average geometry parameters of $Si_{192}H_{16}$ are shown in Figure 1a. The optimized diameter of the $Si_{192}H_{16}$ structure is 10.61 Å and the average Si-Si bond length is 2.29 Å (see Supplementary Material S.3) which is in agreement with the results obtained by Barnard and Russo (Costero et al., 2007), smaller than in cubic diamond crystal form (Uemoto et al., 2019), thus validating our level of calculation. The Si-Si bond order shows a characteristic of covalent bonds between Si atoms, with average value of 1.10. The Si-Si-Si bond angles are characterized as a mixture of $sp^3$-$sp^2$ hybridization, averaging approximately 115.96°, in a range of 103.42° and 125.95°. These values are in agreement with bond angles of

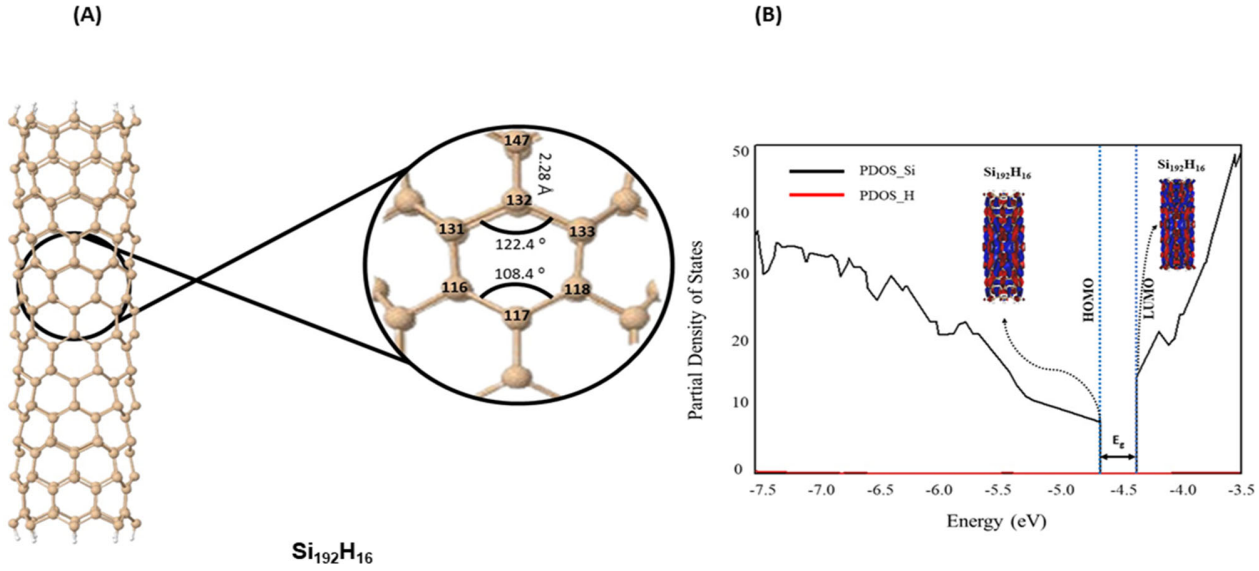


Figure 1. $Si_{192}H_{16}$ Model Optimized in DFT//B3LYP/6-31G* with Grimme GD3 correction. (A) Model and geometric parameters. (B) Density of States with the partial contribution of each atom to the $Si_{192}H_{16}$.

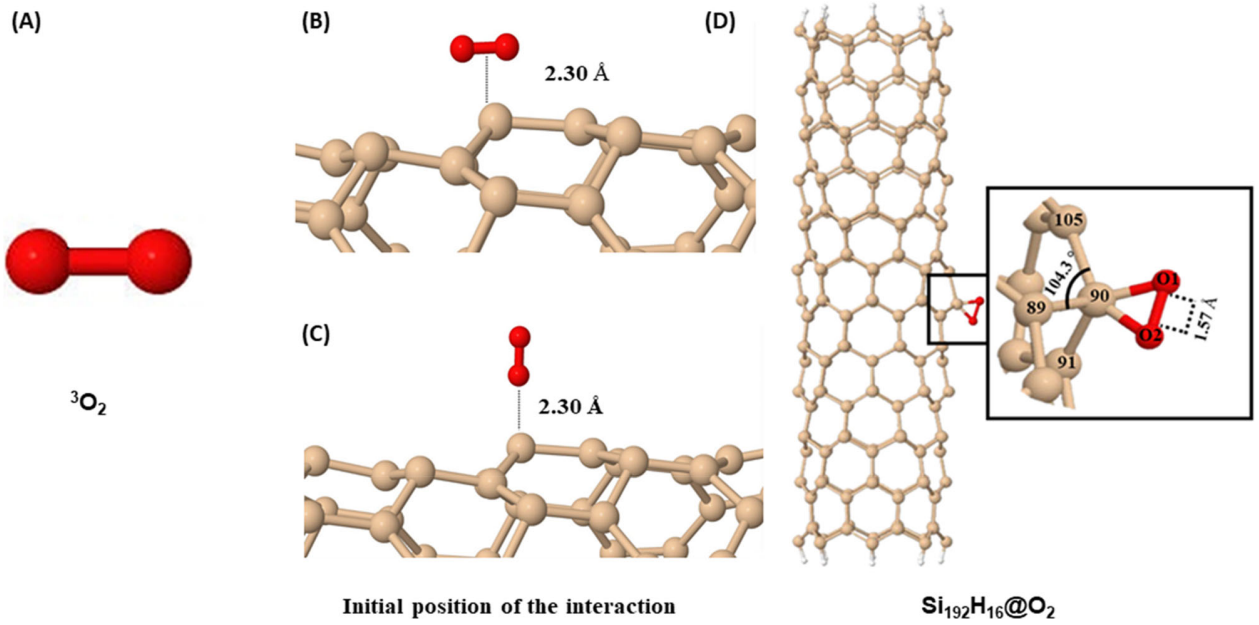


Figure 2. (A) triplet molecular oxygen model optimized in DFT//B3LYP/6-31G* (B-C) Initial position of interaction between $O_2$ and the $Si_{192}H_{16}$ surface. (D) Optimization parameter in the chemisorption region.

$sp^3$ (109.5°) and $sp^2$ (120.0°) hybridizations, respectively (see Supplementary Material S.3). This hybridization mixture is in accordance with the experimental results found by Crescenzi *et al.* (De Crescenzi et al., 2005). Although the edge states are not fully passive, a problem that is common for finite length molecular nanotubes, partial density of states (PDOS) analysis (see Figure 1) shows that saturation with hydrogen atoms at the terminal atoms, a method that avoids edge effects, thus reducing free valances, has no significant influence on the valence and or conduction bands, thus evidencing that the methodology is effective.

The reactivity parameters of $Si_{192}H_{16}$ were based on the energies of the molecular orbitals (HOMO and LUMO). For instance, according to the Koopmans' theorem (Koopmans, 1934), the ionization potential (IP) can be described by the negative of the HOMO energy, and the electronic affinity (EA) can be approximated by the negative of the LUMO energy. The band gap energy ($E_g$) is another important property obtained from these energies. Large and small values of $E_g$ imply high stability and high reactivity, respectively, of a compound in a chemical reaction, as well as assisting in the process of electronic characterization of the material. The $E_g$ value (0.29 eV, Table 1) shows that $Si_{192}H_{16}$ can be treated as a semiconductor material. In addition, this low value implies that the $Si_{192}H_{16}$ has high chemical reactivity. These characteristics make the surfaces of silicon nanotubes promising for functionalization, as well as excellent candidates for antiviral surfaces

Table 1. Electronic properties of the $^3O_2$, $H_2O$, $Si_{192}H_{16}$, $Si_{192}H_{16}@O_2$ and $Si_{192}H_{16}@O_2H$-OH models obtained from DFT-GD3//B3LYP/6-31G (d).

| | Compounds | | | | |
|---|---|---|---|---|---|
| Properties[a] | $^3O_2$ | $H_2O$ | $Si_{192}H_{16}$ | $Si_{192}H_{16}@O_2$ | $Si_{192}H_{16}@O_2H@OH$ |
| E | −94324.81 | −47934.02 | −34884616.31 | −34978964.80 | −35026950.48 |
| G | −94334.97 | −47931.83 | −34884534.30 | −34978883.80 | −35026855.70 |
| H | −94320.36 | −47918.37 | −34884132.27 | −34978473.87 | −35026441.72 |
| ΔG | – | – | – | −14.53 | −40.07 |
| ΔH | – | – | – | −21.24 | −49.48 |
| $E_{ad}$ | – | – | – | −23.68 | – |
| $E_{form}$ | – | – | – | – | −51.63 |
| $E_{HOMO}$ | −8.34 | −7.92 | −4.66 | −4.88 | −4.70 |
| $E_{LUMO}$ | 5.34 | 1.70 | −4.37 | −4.39 | −4.34 |
| $E_g$ | 13.68 | 9.62 | 0.29 | 0.49 | 0.36 |
| IP | 8.34 | 7.92 | 4.66 | 4.88 | 4.70 |
| EA | −5.43 | −1.70 | 4.37 | 4.39 | 4,34 |
| μ | – | 2.10 | 0.01 | 8.36 | 2.02 |

[a]Where 'E' is the Energy of the system, 'G' is the Gibbs free energy, 'H' is the enthalpy, $E_g = |E_{HOMO} - E_{LUMO}|$. The properties: E, G, H, ΔG, ΔH, $E_{ad}$ and $E_{form}$ in kcal/mol. The properties: $E_{HOMO}$, $E_{LUMO}$, $E_g$, IP and EA in eV. The dipole moment (μ) in Debye.

### 3.2. Adsorption of $O_2$ triplet molecules on SiNT (8.0) surface

As mentioned before, several starting positions (different angles) for the adsorption of molecular oxygen ($^3O_2$) on the $Si_{192}H_{16}$ surface were considered in the central regions, thus avoiding as much as possible interferences caused by finite ends, as shown in Figure 2a and Figure 2c. The optimized $^3O_2$ has a bond angle of 180.0° and O1-O2 bond length of 1.21 Å as shown in Figure 2a. Each oxygen atom has 2 half-filled p-type atomic orbitals, where an overlap of atomic orbitals occurs, giving rise to a lower energy triplet state, where 2 electrons are unpaired, occupying two degenerate molecular levels.

For $^3O_2$ specie, a stable chemisorption configuration is found (see Figure 2d), where oxygen atom binds covalently with silicon atom keeping bond order of 0.96 and 0.56 for Si90-O1 and Si90-O2 bonds, respectively. The bond distance between Si and O atoms are 1.67 and 1.75 Å for Si-O1 and Si-O2, respectively. The adsorption energy, obtained from equation 1 is −23.68 kcal/mol, and the variations of Gibbs free energy and enthalpy under standard conditions of temperature and pressure - CNTP (298.15 K and 1 atm), indicate that the adsorption process is a chemical process and that the reaction is exothermic. The reactivity, energetic and electronic parameters calculated for the $Si_{192}H_{16}@O_2$ complex are summarized in Table 1.

For the most stable adsorption configuration, the silicon atom that makes up the Si-O2 interaction, is pulled slightly out of the sidewall. Thus, the neighboring Si-Si bonds are slightly altered, for example, the Si-Si bonds that were once 2.28 Å become 2.36 Å for Si-Si (O2) and 2.46 Å for Si-Si (O1), causing the local Si hybridization to resemble a $sp^3$ hybridization, assuming a bond angle of 104.3° (see Figure 2d). It is worth noting that this minimal elongation in the local bonds and consequently definition of local hybridization, do not cause drastic changes in the tubular geometry of the model, since it already has characteristics of hybridization mixing. It is still worth noting that the interaction of $^3O_2$ with the surface of $Si_{192}H_{16}$, also causes a significant increase in the O1-O2 bond to 1.57 Å, thus suggesting a charge transfer between $Si_{192}H_{16}$ and the adsorbed $O_2$ molecular. Analysis of the atomic charges indicates that the charge transfer is approximately 0.70 e- from the nanotube to the oxygen atoms.

Since there are effective charge transfers, the analysis of the Map Electrostatic Potential (MEP) is of paramount importance. The MEP measures the interaction of a positively charged point with nuclei and electrons of the same compound. MEP's result from the electrostatic potential over the electron density, using a color scale from red to blue to represent the potential values. Colors that tend toward "red" indicate negative values of the electrostatic potential, while colors that tend toward "blue" indicate positive values of the potential. Analyzing the MEP's, we can observe that the surface of pure $Si_{192}H_{16}$ possessed a slightly nucleophilic character (Figure 3a) before the interaction with $^3O_2$ and after the chemisorption of $^3O_2$ the surface of $Si_{192}H_{16}$ came to possess a slightly electrophilic character (Figure 3b). This fact can be evidenced by the small increase in electronic affinity from 4.37 eV to 4.39, assuming a percentage increase of approximately 0.46%. This small change in character allows $Si_{192}H_{16}$, now with positive character, to function as an electron receptor surface, thus enabling a new functionalization. Furthermore, the analysis of the contribution of each atom in the density of states (PDOS) shows that $^3O_2$ has a small contribution in the valence band in the energy range of −6.6 to −5.5 eV, making the HOMO region more centralized (see Figure 4). This small contribution causes the LUMO region to concentrate on the surface Si atoms, making them electron acceptors.

### 3.3. Interaction of $Si_{192}H_{16}@O_2$ with $H_2O$

Considering the new electronic properties, provided by the oxidation of the $Si_{192}H_{16}$ surface, the interaction of $H_2O@Si_{192}H_{16}@O_2$ in the regions near the oxidation was evaluated (see Figure 5a). For the adsorption of $H_2O$ in the regions near the adsorbed $O_2$ molecule, a more stable configuration is found. According to the bond length and bond order analysis of 1.70 Å and 0.90, respectively, the values point out that the oxygen from $H_2O$ covalently binds to Si105 after the surface receives electronic density from water.

The structural analysis of $Si_{192}H_{16}@O_2H$-OH shows that the addition of the (-$O_2$H) and (-OH) groups on the surface of

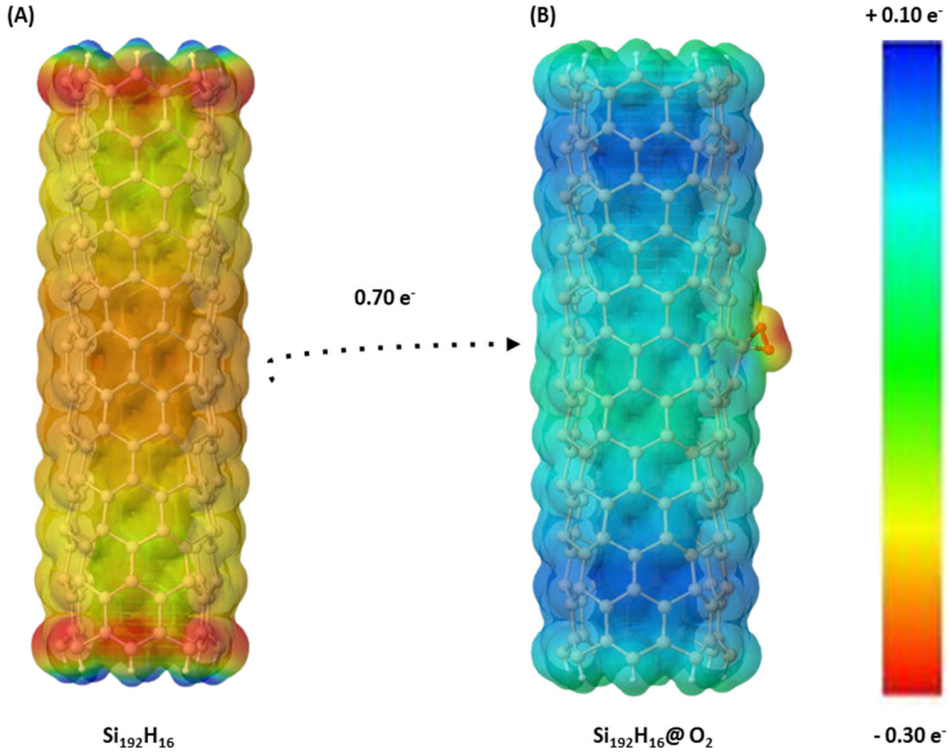


Figure 3. Map Electrostatic potential (MEP) at a distance of 1.4 Å. (A) Electrostatic potential surface for $Si_{192}H_{16}$. (B) Electrostatic potential surface for $Si_{192}H_{16}@O_2$.

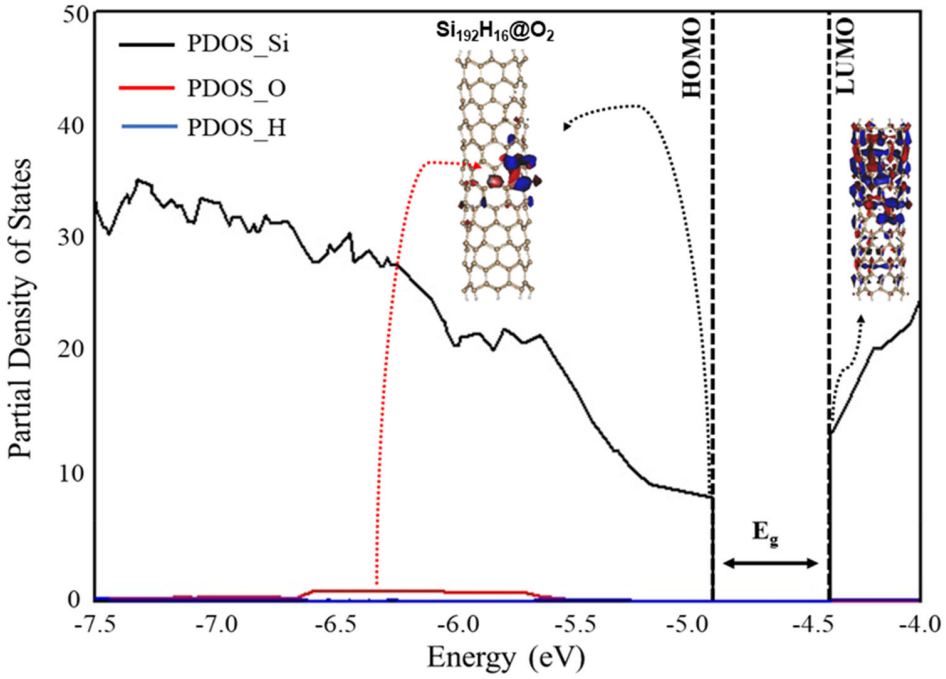


Figure 4. Density of States with the partial contribution of each atom to the $Si_{192}H_{16}@O_2$.

$Si_{192}H_{16}$ does not damage the tubular geometric structure of the compound. Minor modifications are found in the interaction region such as increasing the Si109-Si90 bond length from 2.26 to 2.39 Å. Minor modifications in the bond angles and dihedral angles were also observed, causing the Si105 and Si90 atoms to project slightly out of plane forming polygons with the Si106, Si120, Si89 and Si91 atoms (see Supplementary Material S.4).

Analysis of the atomic charges indicates that the electron transfer from $H_2O$ to the nanotube is approximately 0.44 $e^-$.Therefore, due to these charges transfer from $H_2O$ to the $Si_{192}H_{16}$, the water and SiNT acts as reducing and oxidizing agents, respectively. Contrary, the $Si_{192}H_{16}$ acts as a reducing agent in the $O_2$ adsorption process, in which 0.70 $e^-$ are transferred from $Si_{192}H_{16}$ to $O_2$ (see section 3.2).In the electron transfer process, the bond length between O3-H5 gives

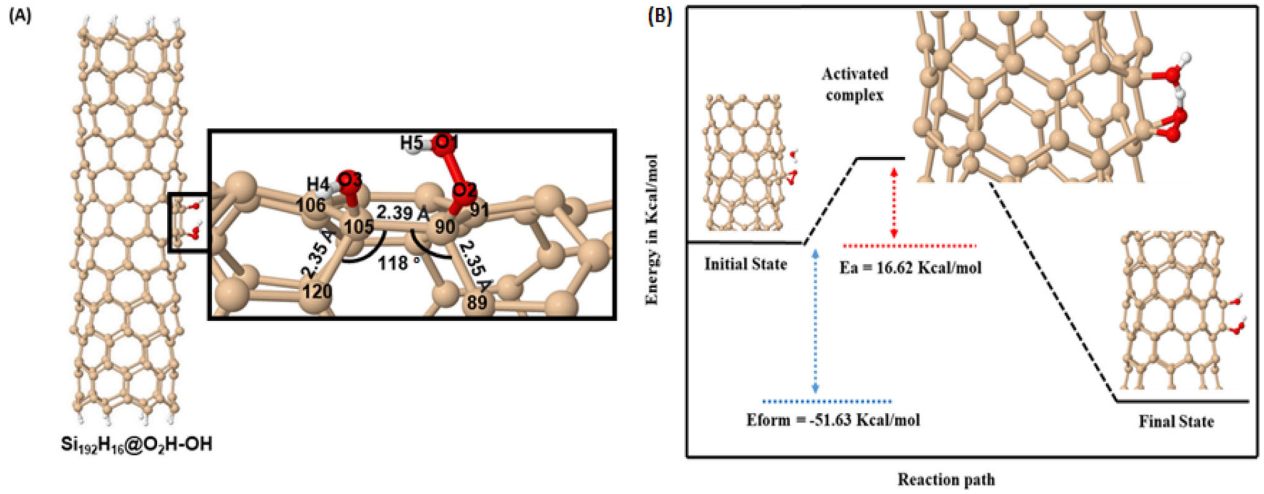


Figure 5. Interaction between $H_2O$ and the $Si_{192}H_{16}@O_2$ model (A) Structural changes. (B) Energetic changes in the reaction path.

$H_2O$ increases and the O3-Si105 bond is formed, and in the interim an activated complex with Activation Energy (Ea) of 16.62 kcal/mol is formed, as can be seen in Figure 5b. After the formation of the activated complex, characterized by a point of maximum energy, the formation of the compound $Si_{192}H_{16}@O_2H$-OH occurs, where this formation is characterized by a point of minimum energy (see Figure 5b). The energy of formation was obtained using equation 2 and is approximately −51.63 kcal/mol. This value, together with the values of Gibbs free energy variation and enthalpy at CNTP indicate that the formation of the $Si_{192}H_{16}@O_2H$-OH compound is chemical in nature, exothermic and spontaneous (see Table 1).

To evaluate the effectiveness of the functionalization, the removal energy (Er) of the $O_2H$ and OH groups from the surface at a distance of 2.29 Å was calculated using equation 3.

$$E_r = E_{\frac{SiNT}{O}2\frac{H}{OH}} - E_{SiNT@O2H-OH} \quad (3)$$

where $E_r$ is the removal energy of the $O_2H$ and OH groups, $E_{\frac{SiNT}{O}2\frac{H}{OH}}$ is the total energy of the $Si_{192}H_{16}$//$O_2H$//OH system at a distance of 2.29 Å, and $E_{SiNT@O2H-OH}$ is the total energy of the $Si_{192}H_{16}@O_2H$-OH compound.

The positive value of the removal energy indicates that the process of separation of $O_2H$ and OH groups from the $Si_{192}H_{16}$ surface is not energetically favorable, thus requiring an energy of 77.58 kcal/mol. Besides energetically ensuring the effectiveness of the functionalization, O2H and OH groups must be retained on the surface for a long time to be useful in viral capture/inactivation. Thus, the recovery time was calculated using conventional transition state theory and can be expressed by equation (4) (Aasi et al., 2020; Pitt et al., 1994).

$$t = \nu_0^{-1} \frac{\exp^{-E}_{form}}{K_B T} \quad (4)$$

where $\upsilon_0$ is the tentative frequency, $E_{form}$ is the formation energy of the $Si_{192}H_{16}@O_2H$-OH compound, T is the temperature, and $K_B$ is the Boltzmann constant.

It is expected that at constant temperature, small adsorption energy results in a rapid desorption process of the groups. The recovery time obtained for the desorption of $O_2H$ and OH groups from the surface at room temperature under UV radiation ($\nu_0$ = 1016 Hz) and temperature 298.15 K is approximately $7.3 \times 10^{21}$ seconds. The long recovery time obtained for $Si_{192}H_{16}$ after functionalization ($2.3 \times 10^{14}$ years) suggests that the $Si_{192}H_{16}@O_2H$-OH system has excellent potential for virus removal materials with a very long lifetime. Furthermore, the results obtained here indicate that silicon nanotube surfaces functionalized with $O_2H$ and OH may be more promising than carbon nanotube surfaces decorated with transition metals (Pt, Rh, Ru and Cu) functionalized with $H_2O_2$, since, the best results found by Aref Aasi *et al.* for SWNCT-$H_2O_2$ systems decorated with Pt and Cu are $2.2 \times 10^{12}$ and $1.9 \times 10^{8}$ years, respectively (Aasi et al., 2020), an order of magnitude 100 times smaller than that obtained by the $Si_{192}H_{16}@O_2H$-OH system.

### 3.4. Molecular docking

In the docking calculations, the interaction energy between the best docking SiNTs ($Si_{192}H_{16}$ and $Si_{192}H_{16}@O_2H$-OH) with S-protein were favorable with binding energy of −11.83 (with inhibition constant of 2.13 nM) and −11.13 (with inhibition constant of 6.99 nM) kcal/mol, respectively. This shows that $Si_{192}H_{16}$ binds more strongly to S-protein than $Si_{192}H_{16}@O_2H$-OH. Figure 6 shows the nanotubes with lower interaction energy docked on the S-protein.

In Figure 6 we can observe that the $Si_{192}H_{16}$ and $Si_{192}H_{16}@O_2H$-OH nanotubes bind similarly in the same region of the S-protein. It is worth noting that in Figure 6c, ACE2 (in yellow) was only considered to improve the visualization of the binding site of the nanotubes obtained in the docking calculations. For $Si_{192}H_{16}@O_2H$-OH no specific interaction between the OH and $O_2H$ groups with the amino acids of the S-protein was observed. Both nanotubes interacted with the following amino acids of S-protein at a cut-off radius of 4.0 Å: Val445, Gly446, Gln498, Thr500, Thr415, Gly416, Lys417, Tyr421, Lys458, Ser459, Asn460, Tyr473, Ala475, Gly476 and Ser477. Among these residues, the

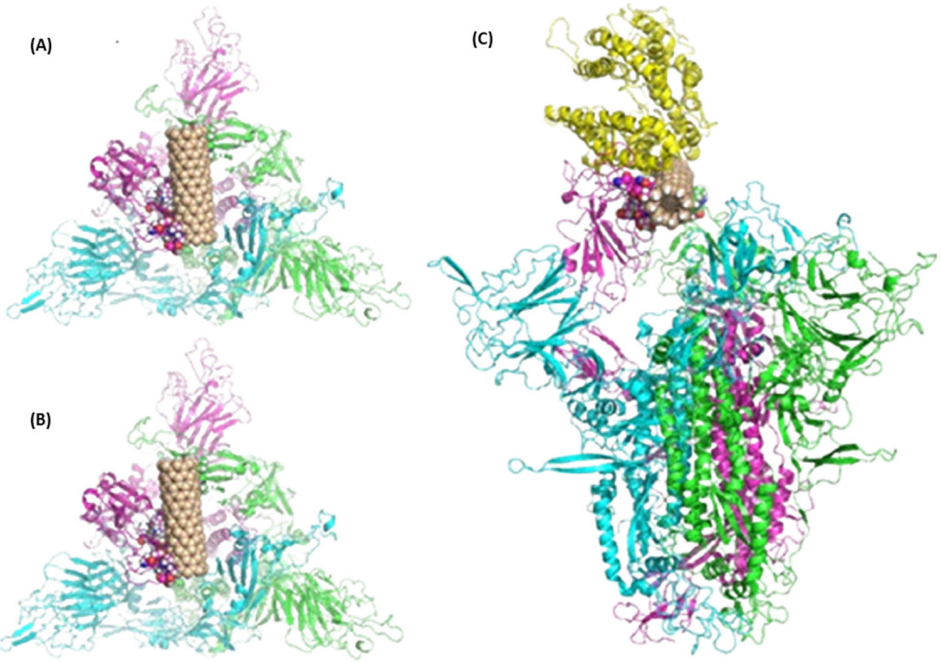


Figure 6. Best data obtained from docking calculations. (A) SiNT@S-protein, (B) SiNT-OH-O2H@S-protein and (C) nanotubes@S-protein in the presence of ACE2 (yellow color).

Lys417, Tyr473, Ala475, and Gly476 interact with the amino acids Ser19, Thr27 and Asp30 of the ACE2 enzyme at a cut-off radius 4.0 Å. Therefore, the present nanotubes can inhibit S-protein by two mechanisms: i) oxidation of S-protein amino acids and ii) preventing effective interaction (due to steric hindrance) between S-protein and human ACE2. Finally, ADMET (absorption, distribution, metabolism, excretion, and toxicity) properties obtained from the DataWarrior program (Sander et al., 2015) show that the present nanotubes are not mutagenic and tumorigenic with a water solubility (clogS) of −0.53.Therefore, SiNT may have low water solubility due to its high symmetry. Moreover, as shown in our docking calculations. The SiNT binds favorably with the S-protein. Therefore, we believe that the SiNT pure and the SiNT- Sprotein complex can be released from the human body in an expontaneous process in a non-toxic manner.

## 4. Conclusions

COVID-19 is a disease that originated in Wuham in late 2019 and the pandemic was declared in March 2020. This disease is caused by SARS-CoV-2 virus. Due to the emergency in obtaining compounds that can combat the virus, herein we propose the use of $Si_{192}H_{16}$ nanotube as a possible virucidal agent. In this way, this nanotube and its functionalization with $^3O_2$ and $H_2O$ ($H_2O@Si_{192}H_{16}@O_2$) were studied using quantum chemistry and molecular docking methods. The structural parameters obtained by DFT are in agreement with those reported in the literature. The electronic results show that the nanotube is energetically favorable with negative Gibbs free energy. Also, the nanotube presents properties of a semiconductor with an energy gap of 0.29 eV, which implies its high reactivity towards chemical reactions. In the functionalization process, the formation energy and activation energy were −51.63 and 16.62 kcal/mol, respectively, and the Gibbs free energy was also favorable for the $H_2O@Si_{192}H_{16}@O_2$. The recovery time calculated for the desorption of $O_2H$ and OH groups from the surface is approximately $7.3 \times 10^{21}$ seconds. Whereas, the long recovery time obtained for $Si_{192}H_{16}$ after functionalization ($2.3 \times 10^{14}$ years) suggests that the $Si_{192}H_{16}@O_2H$-OH system has excellent potential for virus removal materials with a long lifetime. On the other hand, molecular docking calculations showed that the $Si_{192}H_{16}$ and $Si_{192}H_{16}@O_2H$-OH nanotubes bind favorably on the SARS-CoV-2 S-protein with binding energy of −11.83 and −11.13 kcal/mol, respectively. Therefore, the functionalized nanotubes will interact with the amino acids of the S-protein by inactivating them. Overall, the results obtained here indicate that the $Si_{192}H_{16}$ nanotube is a potential candidate for use against COVD-19 via reacting with S-protein and/or steric hindrance avoiding the formation of the S-protein-ACE2 complex.

## Acknowledgements

This research was carried out with the support of the Center for High Performance Computing at the State University of Goiás.

## Disclosure statement

No potential conflict of interest was reported by the authors.

## Funding

Jeziel Rodrigues dos Santos thanks CAPES for providing a research grant.

## ORCID

*Pedro Simão Sousa Mendonça* http://orcid.org/0000-0002-1913-4434
*Jeziel Rodrigues dos Santos* http://orcid.org/0000-0002-3147-4757
*Osmair Vital de Oliveira* http://orcid.org/0000-0001-9463-2567
*José Divino dos Santos* http://orcid.org/0000-0002-9272-414X
*Elson Longo* http://orcid.org/0000-0001-8062-7791

## References

Aasi, A., Aghaei, S. M., Moore, M. D., & Panchapakesan, B. (2020). Pt-, rh-, ru-, and cu-single-wall carbon nanotubes are exceptional candidates for design of anti-viral surfaces: A theoretical study. *International Journal of Molecular Sciences*, *21*(15), 5211–5223. https://doi.org/10.3390/ijms21155211

Allouche, A. (2011). Software news and updates Gabedit — A graphical user interface for computational chemistry softwares. *Journal of Computational Chemistry*, *32*(1), 174–182. https://doi.org/10.1002/jcc https://doi.org/10.1002/jcc.21600

Antônio Pinheiro Lobo, J., Rodrigues dos Santos, J., Vital de Oliveira, O., Longo da Silva, E., & Divino dos Santos, J. (2020). Theoretical study of greenhouse gases on the zirconium oxide nanotube surface. *Chemical Physics Letters*, *745*(February), 137236. https://doi.org/10.1016/j.cplett.2020.137236

Assis, M., Simoes, L. G. P., Tremiliosi, G. C., Coelho, D., Minozzi, D. T., Santos, R. I., Vilela, D. C. B., Santos, J. R., Do Ribeiro, L. K., Rosa, I. L. V., Mascaro, L. H., Andrés, J., & Longo, E. (2021). Sio2-ag composite as a highly virucidal material: A roadmap that rapidly eliminates sars-cov-2. *Nanomaterials*, *11*(3), 19–1. https://doi.org/10.3390/nano11030638

Assis, M., Simoes, L. G. P., Tremiliosi, G. C., Ribeiro, L. K., Coelho, D., Minozzi, D. T., Santos, R. I., Vilela, D. C. B., Mascaro, L. H., Andrés, J., & Longo, E. (2021). PVC-SiO2-Ag composite as a powerful biocide and anti-SARS-CoV-2 material. *Journal of Polymer Research*, *28*(9), 7-1. https://doi.org/10.1007/s10965-021-02729-1

Bai, J., Zeng, X. C., Tanaka, H., & Zeng, J. Y. (2004). Metallic single-walled silicon nanotubes. 2003, 2668–2664.

Berger, S., Faltenbacher, J., Bauer, S., & Schmuki, P. (2008). Enhanced self-ordering of anodic ZrO2 nanotubes in inorganic and organic electrolytes using two-step anodization. *Physica Status Solidi (RRL) – Rapid Research Letters*, *2*(3), 102–104. https://doi.org/10.1002/pssr.200802019

Burwell, R. L. (1966). The mechanism of heterogeneous catalysis. *Chemical & Engineering News Archive*, *44*(34), 56–67. https://doi.org/10.1021/cen-v044n034.p056

Camilli, L., & Passacantando, M. (2018). Advances on sensors based on carbon nanotubes. *Chemosensors*, *6*(4), 17–1. https://doi.org/10.3390/chemosensors6040062

Castrucci, P., Scarselli, M., De Crescenzi, M., Diociaiuti, M., Chaudhari, P. S., Balasubramanian, C., Bhave, T. M., & Bhoraskar, S. V. (2006). Silicon nanotubes: Synthesis and characterization. *Thin Solid Films.*, *508*(1–2), 226–230. https://doi.org/10.1016/j.tsf.2005.07.348

Costero, A. M., Royo, S., Martínez-Máñez, R., Gil, S., Parra, M., & Sancenón, F. (2007). Chromogenic and fluorogenic reagents for chemical warfare nerve agents' detection. *Chemical Communications*, *46*(46), 4839. https://doi.org/10.1039/b707063b

De Crescenzi, M., Castrucci, P., Scarselli, M., Diociaiuti, M., Chaudhari, P. S., Balasubramanian, C., Bhave, T. M., & Bhoraskar, S. V. (2005). Experimental imaging of silicon nanotubes. *Applied Physics Letters*, *86*(23), 231901–231903. https://doi.org/10.1063/1.1943497

De Las Casas, C., & Li, W. (2012). A review of application of carbon nanotubes for lithium ion battery anode material. *Journal of Power Sources*, *208*, 74–85. https://doi.org/10.1016/j.jpowsour.2012.02.013

Dobbs, K. D., & Hehre, W. J. (1986). Molecular orbital theory of the properties of inorganic and organometallic compounds 4. Extended basis sets for third-and fourth-row, main-group elements. *Journal of Computational Chemistry*, *7*(3), 359–378. https://doi.org/10.1002/jcc.540070313

dos Santos, J. R., da Silva, E. L., de Oliveira, O. V., & dos Santos, J. D. (2020). Theoretical study of sarin adsorption on (12,0) boron nitride nanotube doped with silicon atoms. *Chemical Physics Letters*, *738*(October), 136816. https://doi.org/10.1016/j.cplett.2019.136816

Fagan, S. B., Baierle, R., Mota, R., da Silva, A. J. R., & Fazzio, A. (2000). Ab initio calculations for a hypothetical material: Silicon nanotubes. *Physical Review B*, *61*(15), 9994–9996. https://doi.org/10.1103/PhysRevB.61.9994

Frisch,M. J., Caminhoes, G. W., Shlegel, H. B., Scuseria, G. E., Robb, M. A., Cheeseman, J. R., Scalmani, G., Barone, V., Mennucci, B., Petersson, G. A., Nakatsuji, H., Caricoto, M., Li, X., Hratchian, H. P., Izmaylov, A. F., Bloino, J., Zheng, G., Sonnenberg, J. L., Hada, M., ... Fox, D. J., (2009). Gaussian09, Revisão E.01, Gaussian, Inc., Wallingford CT.

Glendening, E. D., Landis, C. R., & Weinhold, F. (2012). Natural bond orbital methods. *WIREs Computational Molecular Science*, *2*(1), 1–42. https://doi.org/10.1002/wcms.51

Gligorovski, S., Strekowski, R., Barbati, S., & Vione, D. (2015). Environmental Implications of Hydroxyl Radicals ((•)OH)). *Chemical Reviews*, *115*(24), 13051–13092. https://doi.org/10.1021/cr500310b

Golberg, D., Bando, Y., Tang, C. C., & Zhi, C. Y. (2007). Boron nitride nanotubes. *Advanced Materials*, *19*(18), 2413–2432. https://doi.org/10.1002/adma.200700179

González-Durruthy, M., Werhli, A. V., Seus, V., Machado, K. S., Pazos, A., Munteanu, C. R., González-Díaz, H., & Monserrat, J. M. (2017). Decrypting strong and weak single-walled carbon nanotubes interactions with mitochondrial voltage-dependent anion channels using molecular docking and perturbation theory. *Scientific Reports*, *7*(1), 1–19. https://doi.org/10.1038/s41598-017-13691-8

Grimme, S., Antony, J., Ehrlich, S., & Krieg, H. (2010). A consistent and accurate ab initio parametrization of density functional dispersion correction (DFT-D) for the 94 elements H-Pu. *Journal of Chemical Physics*, (15), 18-1. https://doi.org/10.1063/1.3382344

Han, T., Nag, A., Chandra Mukhopadhyay, S., & Xu, Y. (2019). Carbon nanotubes and its gas-sensing applications: A review. *Sensors and Actuators A: Physical*, *291*, 107–143. https://doi.org/10.1016/j.sna.2019.03.053

Hayyan, M., Hashim, M. A., & Alnashef, I. M. (2016). Superoxide ion: Generation and chemical implications. *Chemical Reviews*, *116*(5), 3029–3085. https://doi.org/10.1021/acs.chemrev.5b00407

Hirana, Y., Juhasz, G., Miyauchi, Y., Mouri, S., Matsuda, K., & Nakashima, N. (2013). Empirical prediction of electronic potentials of single-walled carbon nanotubes with a specific chirality (n,m). *Scientific Reports*, *3*, 6–1. https://doi.org/10.1038/srep02959

Honda, H., Ishizaki, A., Soma, R., Hashimoto, K., & Fujishima, A. (1998). Application of photocatalytic reactions caused by tio2 film to improve the maintenance factor of lighting systems. *Journal of the Illuminating Engineering Society*, *27*(1), 42–49. https://doi.org/10.1080/00994480.1998.10748209

Hu, D., Zhu, C., Ai, L., He, T., Wang, Y., Ye, F., Yang, L., Ding, C., Zhu, X., Lv, R., Zhu, J., Hassan, B., Feng, Y., Tan, W., & Wang, C. (2018). Genomic characterization and infectivity of a novel SARS-like coronavirus in Chinese bats. *Emerging Microbes & Infections*, *7*(1), 1–10. https://doi.org/10.1038/s41426-018-0155-5

Iijima, S. (1991). Helical microtubules of graphitic carbon. *Nature*, *354*(6348), 56–740. https://doi.org/10.1038/354056a0

Stewart, J. J. (1990). MOPAC: A semiempirical molecular orbital program. *Journal of Computer-Aided Molecular Design*, *4*(1), 1–105.

Jeong, S. Y., Kim, J. Y., Yang, H. D., Yoon, B. N., Choi, S. H., Kang, H. K., Yang, C. W., & Lee, Y. H. (2003). Synthesis of silicon nanotubes on porous alumina using molecular beam epitaxy. *Advanced Materials*, *15*(14), 1172–1176. https://doi.org/10.1002/adma.200304898

Jitianu, A., Cacciaguerra, T., Benoit, R., Delpeux, S., Béguin, F., & Bonnamy, S. (2004). Synthesis and characterization of carbon nanotubes-TiO2 nanocomposites. *Carbon*, *42*(5-6), 1147–1151. https://doi.org/10.1016/j.carbon.2003.12.041

Kampf, G., Todt, D., Pfaender, S., & Steinmann, E. (2020). Persistence of coronaviruses on inanimate surfaces and their inactivation with biocidal agents. *The Journal of Hospital Infection*, *104*(3), 246–251. https://doi.org/10.1016/j.jhin.2020.01.022

Kearns, D. R. (1971). Physical and chemical properties of singlet molecular oxygen. *Chemical Reviews*, *71*(4), 395–427. https://doi.org/10.1021/cr60272a004

Koopmans, T. (1934). Über die Zuordnung von Wellenfunktionen und Eigenwerten zu den Einzelnen Elektronen Eines Atoms. *Physica*, *1*(1–6), 104–113. https://doi.org/10.1016/S0031-8914(34)90011-2

Larsen, J. R., Martin, M. R., Martin, J. D., Kuhn, P., & Hicks, J. B. (2020). Modeling the onset of symptoms of COVID-19. *Frontiers in Public Health*, *8*(August), 473. https://doi.org/10.3389/fpubh.2020.00473

Lissi, E. A., Encinas, M. V., Lemp, E., & Rubio, M. A. (1993). Singlet oxygen O2(1Δg) bimolecular processes. Solvent and compartmentalization effects. *Chemical Reviews*, *93*(2), 699–723. https://doi.org/10.1021/cr00018a004

Lu, N., Sui, Y., Ding, Y., Tian, R., & Peng, Y. Y. (2018). Fibrinogen binding-dependent cytotoxicity and degradation of single-walled carbon nanotubes. *Journal of Materials Science: Materials in Medicine*, *29*(8), 9–13. https://doi.org/10.1007/s10856-018-6123-8

Lu, T., & Chen, F. (2012). Multiwfn: A multifunctional wavefunction analyzer. *Journal of Computational Chemistry*, *33*(5), 580–592. https://doi.org/10.1002/jcc.22885

Ma, J., Ping, D., & Dong, X. (2017). Recent developments of graphene oxide-based membranes: A review. *Membranes*, *7*(3), 52. https://doi.org/10.3390/membranes7030052

Mahdavifar, Z., Abbasi, N., & Shakerzadeh, E. (2013). A comparative theoretical study of CO2 sensing using inorganic AlN, BN and SiC single walled nanotubes. *Sensors and Actuators B: Chemical*, *185*, 512–522. https://doi.org/10.1016/j.snb.2013.05.004

Nosaka, Y., & Nosaka, A. (2016). Understanding hydroxyl radical (•OH) generation processes in photocatalysis. *ACS Energy Letters*, *1*(2), 356–359. https://doi.org/10.1021/acsenergylett.6b00174

Nosaka, Y., & Nosaka, A. Y. (2017). Generation and detection of reactive oxygen species in photocatalysis. *Chemical Reviews*, *117*(17), 11302–11336. https://doi.org/10.1021/acs.chemrev.7b00161

Patel, S., Srivastav, A. K., Gupta, S. K., Kumar, U., Mahapatra, S. K., Gajjar, P. N., & Banerjee, I. (2021). Carbon nanotubes for rapid capturing of SARS-COV-2 virus: Revealing a mechanistic aspect of binding based on computational studies. *RSC Advances*, *11*(10), 5785–5800. https://doi.org/10.1039/D0RA08888A

Pitt, I. G., Gilbert, R. G., & Ryan, K. R. (1994). Application of transition-state theory to gas-surface reactions: Barrierless adsorption on clean surfaces. *The Journal of Physical Chemistry*, *98*(49), 13001–13010. https://doi.org/10.1021/j100100a031

Planeix, J. M., Coustel, N., Coq, B., Brotons, V., Kumbhar, P. S., Dutartre, R., Geneste, P., Bernier, P., & Ajayan, P. M. (1994). Application of carbon nanotubes as supports in heterogeneous catalysis. *Journal of the American Chemical Society*, *116*(17), 7935–7936. https://doi.org/10.1021/ja00096a076

Pokatilov, E. P., Nika, D. L., & Balandin, A. A. (2005). Acoustic-phonon propagation in rectangular semiconductor nanowires with elastically dissimilar barriers. *Physical Review B*, *72*(11), 4–7. https://doi.org/10.1103/PhysRevB.72.113311

Rassolov, V. A., Ratner, M. A., Pople, J. A., Redfern, P. C., & Curtiss, L. A. (2001). 6-31G* basis set for third-row atoms. *Journal of Computational Chemistry*, *22*(9), 976–984. https://doi.org/10.1002/jcc.1058

Röthlisberger, U., Andreoni, W., & Parrinello, M. (1994). Structure of nanoscale silicon clusters. *Physical Review Letters*, *72*(5), 665–668. https://doi.org/10.1103/PhysRevLett.72.665

Sadan, M. B., Houben, L., Enyashin, A. N., Seifert, G., & Tenne, R. (2008). Atom by atom: HRTEM insights into inorganic nanotubes and fullerene-like structures. *Proceedings of the National Academy of Sciences of the United States of America*, *105*(41), 15643–15648. https://doi.org/10.1073/pnas.0805407105

Sander, T., Freyss, J., Von Korff, M., & Rufener, C. (2015). DataWarrior: An open-source program for chemistry aware data visualization and analysis. *Journal of Chemical Information and Modeling*, *55*(2), 460–473. https://doi.org/10.1021/ci500588j

Seifert, G., Köhler, T., Hajnal, Z., & Frauenheim, T. (2001). Tubular structures of germanium. *Solid State Communications*, *119*(12), 653–657. https://doi.org/10.1016/S0038-1098(01)00309-X

Serra, M., Arenal, R., & Tenne, R. (2019). An overview of the recent advances in inorganic nanotubes. *Nanoscale*, *11*(17), 8073–8090. https://doi.org/10.1039/c9nr01880h

Shah, M., Ahmad, B., Choi, S., & Woo, H. G. (2020). Sequence variation of SARS-CoV-2 spike protein may facilitate stronger interaction with ACE2 promoting high infectivity. *Research Square*, 23-1. https://doi.org/10.21203/rs.3.rs-16932/v1

Sharafeldin, I. M., & Allam, N. K. (2017). DFT insights into the electronic properties and adsorption of NO2 on metal-doped carbon nanotubes for gas sensing applications. *New Journal of Chemistry*, *41*(24), 14936–14944. https://doi.org/10.1039/C7NJ03109B

Solimannejad, M., & Noormohammadbeigi, M. (2017). Boron nitride nanotube (BNNT) as a sensor of hydroperoxyl radical (HO2): A DFT study. *Journal of the Iranian Chemical Society*, *14*(2), 471–476. https://doi.org/10.1007/s13738-016-0994-8

Soltani, A., Peyghan, A. A., & Bagheri, Z. (2013). H2O2 adsorption on the BN and SiC nanotubes: A DFT study. *Physica E: Low-Dimensional Systems and Nanostructures*, *48*, 176–180. https://doi.org/10.1016/j.physe.2013.01.007

Song, T., Xia, J., Lee, J. H., Lee, D. H., Kwon, M. S., Choi, J. M., Wu, J., Doo, S. K., Chang, H., Park, W., Il, Zang, D. S., Kim, H., Huang, Y., Hwang, K. C., Rogers, J. A., & Paik, U. (2010). Arrays of sealed silicon nanotubes as anodes for lithium ion batteries. *Nano Letters*, *10*(5), 1710–1716. https://doi.org/10.1021/nl100086e

Stewart, J. J. P. (2013). Optimization of parameters for semiempirical methods VI: More modifications to the NDDO approximations and re-optimization of parameters. *Journal of Molecular Modeling*, *19*(1), 1–32. https://doi.org/10.1007/s00894-012-1667-x

Uemoto, M., Kuwabara, Y., Sato, S. A., & Yabana, K. (2019). Nonlinear polarization evolution using time-dependent density functional theory. *Journal of Chemical Physics*, *150*(9), 11-1. https://doi.org/10.1063/1.5068711

Wang, R., Xie, L., Hameed, S., Wang, C., & Ying, Y. (2018). Mechanisms and applications of carbon nanotubes in terahertz devices: A review. *Carbon*, *132*, 42–58. https://doi.org/10.1016/j.carbon.2018.02.005

Wolfe, N. D., Dunavan, C. P., & Diamond, J. (2007). Origins of major human infectious diseases. *Nature*, *447*(7142), 279–283. https://doi.org/10.1038/nature05775

Wu, F., Zhao, S., Yu, B., Chen, Y. M., Wang, W., Song, Z. G., Hu, Y., Tao, Z. W., Tian, J. H., Pei, Y. Y., Yuan, M. L., Zhang, Y. L., Dai, F. H., Liu, Y., Wang, Q. M., Zheng, J. J., Xu, L., Holmes, E. C., & Zhang, Y. Z. (2020). A new coronavirus associated with human respiratory disease in China. *Nature*, *579*(7798), 265–269. https://doi.org/10.1038/s41586-020-2008-3

Yang, B., Chen, Y., & Shi, J. (2019). Reactive oxygen species (ROS)-based nanomedicine. *Chemical Reviews*, *119*(8), 4881–4985. https://doi.org/10.1021/acs.chemrev.8b00626

Yang, X., & Ni, J. (2005). Electronic properties of single-walled silicon nanotubes compared to carbon nanotubes. *Physical Review B*, *72*(19), 1–5. https://doi.org/10.1103/PhysRevB.72.195426

Yoo, J. K., Kim, J., Jung, Y. S., & Kang, K. (2012). Scalable fabrication of silicon nanotubes and their application to energy storage. *Advanced Materials (Deerfield Beach, Fla.)*, *24*(40), 5452–5456. https://doi.org/10.1002/adma.201201601

Zhang, W., Zhang, Z., & Zhang, Y. (2011). The application of carbon nanotubes in target drug delivery systems for cancer therapies. *Nanoscale Research Letters*, *6*(1), 1–22. https://doi.org/10.1186/1556-27 https://doi.org/10.1186/1556-276X-6-555